Enceladus might vary markedly by nearly an order of magnitude on time scales of hours (*19*). Jurac *et al.* (*21*) also suggested that impacts by E-ring particles, a possible source, would be insufficient to produce this amount. Nevertheless, Roddier *et al.* (*22*) had imaged a transient feature with HST that could have been interpreted as a large, impact-produced vapor cloud. The fresh deposits on Enceladus' surface suggested by its high albedo also reinforced the idea that E-ring grains are constantly being swept up, along with any larger objects that may be present. Sputtering of ice by energetic O^+ ions as a source required more surface area than could be accounted for by the combination of Enceladus and the expected E-ring grains. In a subsequent paper, Jurac and Richardson (*23*) concluded that the source rate for the observed water needed to be three times larger and that its production mechanism remained unclear. The discovery by Cassini of an unexpected venting of water vapor from the south pole of Enceladus, of approximately the right amount, may provide a solution to this mystery.

References and Notes

1. J. H. Waite *et al.*, *Space Sci. Rev.* **114**, 113 (2005).
2. W. K. Kasprzak *et al.*, *Proc. SPIE* **2803**, 129 (1996).
3. W. H. Press, B. P. Flannery, S. A. Teukolsky, W. T. Vetterling, *Numerical Recipies* (Cambridge Univ. Press, Cambridge, 1986).
4. F. Spahn *et al.*, *Science* **311**, 1416 (2006).
5. J. R. Spencer *et al.*, *Science* **311**, 1401 (2006).
6. C. C. Porco *et al.*, *Science* **311**, 1393 (2006).
7. R. H. Brown *et al.*, *Science* **311**, 1425 (2006).
8. The VIMS-derived mixing ratio is based on the absence of CO absorption features in the gas column between the surface above the south polar cap and the spacecraft (10^{14} cm^{-2}), divided by the column density of water acquired by UVIS during a stellar occultation (1.5×10^{16} cm^{-2}) (*10*).
9. The absence of CO ultraviolet absorption bands in the UVIS occultation data sets an upper limit for CO abundance at 2% of the water density for a measured water column of 1.5×10^{16} cm^{-2} (*10*).
10. C. J. Hansen *et al.*, *Science* **311**, 1422 (2006).
11. S. W. Squyres, R. T. Reynolds, P. M. Cassen, S. J. Peale, *Icarus* **53**, 319 (1983).
12. J. P. Emery, D. M. Burr, D. P. Cruikshank, R. H. Brown, J. B. Dalton, *Astron. Astrophys.* **435**, 353 (2005).
13. D. P. Cruikshank *et al.*, *Icarus* **175**, 268 (2005).
14. S. Boone, M. F. Nicol, in *LPSC 21 Proc.* (Lunar and Planetary Institute, Houston, TX, 1991), pp. 603–610.
15. D. C. Bockelee-Morvan, J. Crovisier, M. J. Mumma, H. A. Weaver, in *Comets II*, M. C. Festou, H. U. Keller, H. A. Weaver, Eds. (Univ. Arizona Press, Tucson, AZ, 2004), pp. 391–423.
16. The observed asymmetries and the coincidence of water vapor, CO_2, and dust appearing to emanate from the south polar tiger stripes region of Enceladus indicate a possible cometary activity analog. Our analysis of the composition and plume shape suggests the temperature below the surface at the source of the water vapor must be somewhere in the range of at least ~190 to 273 K, the temperatures required for the sublimation of ice. If dust particles have been ejected from the cracks in the surface by the action of the flow of water molecules, then it is likely that the confined volume below the surface must be rather small so as to yield sufficiently high gas densities to achieve substantial dust entrainment (*24*). If the observed dust particles are ice condensates from the gas plumes emanating from the cracks, as has also been suggested for comets (*25*), then gas densities must also be quite high. In an expanding cometary coma, the number density of water molecules in which dust is effectively accelerated by the gas flow is greater than about 10^8 cm^{-3}. Near the nucleus, where the dust acceleration is the largest, gas densities are larger than 10^{11} cm^{-3} for a moderately bright comet like 1P/Halley or 1996 B2 (Hyakutake) (*25*). Taken together, this implies that the water flow exits from relatively small fissures in the surface [such as the tiger stripes (2 by 120 km) (*6*) themselves compared with the size of the general emitting region] and that the flow is already accelerated to rather large speeds and is correspondingly cooled below the reservoir temperature [in excess of 190 K (*26*)] when it passes through the surface. The fissures must also be large enough to allow at least semicollisional gas flow below the surface (i.e., the fissure's bore size must be larger than the mean free path between molecules). If the fissures are too small, then molecules will stick to the cold surfaces and never exit, sealing off the crack. Even the average temperature observed by the Composite Infrared Spectrometer of 140 K is far below the sublimation temperature so that most molecules striking the surface would stick. Such recondensation is a common feature included in porous subsurface cometary nucleus models (*27*).
17. M. R. Combi, *Icarus* **123**, 207 (1996).
18. The source strength inferred from the model allows us to estimate a surface density that can be compared to the UVIS observations (*10*) if we assume a thermal escape speed and an area of the outgassing. ISS (*6*) indicates that the tiger stripes region of ice crystal and dust generation presents 1 to 3% of the area of the polar cap at southern latitudes greater than 82°. If we assume that the gas production and dust and ice generation regions coincide, and if we further assume a thermal speed for the water vapor of 400 m s^{-1}, we derive an inferred near-surface density based on the extended plume measured by INMS of 1×10^9 to 5×10^9 cm^{-3}. On the other hand, UVIS (*10*) reports a water column density of 1.5×10^{16} cm^{-2} and infers a scale length of 80 km, which leads to a near-surface density of 1.9×10^9 cm^{-3}. This value is within the range inferred by INMS.
19. L. W. Esposito *et al.*, *Science* **307**, 1251 (2005).
20. D. E. Shemansky, P. Matherson, D. T. Hall, T. M. Tripp, *Nature* **363**, 329 (1993).
21. S. Jurac *et al.*, *Geophys. Res. Lett.* **29**, 2172 (2002).
22. C. Roddier, F. Roddier, J. E. Graves, M. J. Northcott, *Icarus* **136**, 50 (1998).
23. S. Jurac, J. D. Richardson, *J. Geophys. Res.* **110**, 10.1029/2004JA010635 (2005).
24. R. V. Yelle, L. A. Soderblom, J. R. Jokipii, *Icarus* **167**, 30 (2004).
25. T. Yamamoto, O. Ashihara, *Astron. Astrophys.* **152**, L17 (1985).
26. M. R. Combi, W. M. Harris, W. H. Smyth, in *Comets II*, M. C. Festou, H. U. Keller, H. A. Weaver, Eds. (Univ. Arizona Press, Tucson, AZ, 2004), pp. 523–552.
27. B. Davidsson, Y. Skorov, *Icarus* **168**, 163 (2004).
28. The Cassini INMS investigation is supported by contract number 1228303 from the NASA Jet Propulsion Laboratory. M.R.C. was supported by grant NAG5-12822 from the NASA Planetary Atmospheres Program. W.-H.I. was supported by grant NSC 94-2111-M-008-033.

REPORT

Enceladus' Water Vapor Plume

Candice J. Hansen,[1]* L. Esposito,[2] A. I. F. Stewart,[2] J. Colwell,[2] A. Hendrix,[1] W. Pryor,[4] D. Shemansky,[3] R. West[1]

The Cassini spacecraft flew close to Saturn's small moon Enceladus three times in 2005. Cassini's UltraViolet Imaging Spectrograph observed stellar occultations on two flybys and confirmed the existence, composition, and regionally confined nature of a water vapor plume in the south polar region of Enceladus. This plume provides an adequate amount of water to resupply losses from Saturn's E ring and to be the dominant source of the neutral OH and atomic oxygen that fill the Saturnian system.

The youthful geologic appearance of Enceladus (*1*) and the correlation of the peak density of Saturn's E ring with the orbit of Enceladus (*2*) have long led scientists to speculate that Enceladus is the source of the ring (*2–5*). The narrow size distribution of particles in the E ring suggests a liquid or vapor origin, in contrast to the broad range of particle sizes that would be generated by impacts (*2*). To test the hypothesis that Enceladus has geologic activity supplying the E ring as well as neutral species in Saturn's magnetosphere, the Cassini Ultraviolet Imaging Spectrograph (UVIS) team planned stellar occultation observations on Cassini's first and third close flybys of Enceladus to search for the presence of a tenuous atmosphere (*6*). The detection, by the Cassini Magnetometer team (*7*), of draped field lines consistent with the presence of an atmosphere gave further impetus to the second occultation observation. Because of Enceladus' small size and weak gravity (~12 cm/s^2), any sputtered or sublimated atmosphere will be lost (*8*); thus, if a tenuous atmosphere were to be detected, it would have to come from some sort of geologic activity. We now know that

[1]Jet Propulsion Laboratory/California Institute of Technology, 4800 Oak Grove Drive, Pasadena, CA 91109, USA. [2]Laboratory for Air and Space Physics (LASP), University of Colorado, Boulder, CO 80303, USA. [3]Space Environment Technologies, 320 North Halstead, Suite 170, Pasadena, CA 91107, USA. [4]Central Arizona College, Coolidge, AZ 85228, USA.

*To whom correspondence should be addressed. E-mail: Candice.j.Hansen@jpl.nasa.gov

this is the case, and we report here on the results established by the occultations observed by UVIS.

Observations of stellar occultations are a sensitive method for looking for the presence of tenuous atmospheres (9), particularly at ultraviolet wavelengths, where many gases have strong absorptions. The Cassini UVIS has four optical channels: the high-speed photometer (HSP), the extreme ultraviolet (EUV) spectrograph, the far ultraviolet (FUV) spectrograph, and the hydrogen/deuterium absorption cell (6). The HSP and FUV were used to observe the occultations. The HSP is sensitive to 1100 to 1900 Å and is read out once per 2 ms. The FUV also covers the range from 1100 to 1900 Å and was configured with 512 spectral bins (1.56 Å resolution) for the July occultation observation. The FUV integration time was 5 s.

The star lambda Scorpii (Shaula) was occulted by Enceladus on 17 February 2005, the first of three close Enceladus flybys (Fig. 1A). A second occultation, of the star gamma Orionis (Bellatrix), was observed on the third and closest flyby on 14 July 2005 (Fig. 1, B to D). Only the gamma Orionis ingress showed the attenuation of starlight due to the presence of an absorbing gas. No detectable change of signal was detected by the HSP or FUV on the lambda Scorpii occultation before or after the star's signal was blocked by Enceladus. Detection and nondetections and ingress and egress locations are summarized in Table 1.

In the HSP and FUV data for the gamma Orionis occultation ingress, which occurred at −76° latitude, the signal was attenuated as the star passed behind Enceladus' plume (Fig. 2). The starlight started to decrease at ∼24 s before ingress, at a ray altitude of ∼155 km. The signal of the star was lost completely at UTC 19:54:56, when the star crossed behind the hard limb. The HSP has a finite recovery time on bright stars such as gamma Orionis, so it is not possible to separate a weak atmospheric signal from the instrument response on egress. For egress measurements, we summed the FUV spectral pixels, but the temporal resolution is lower than the HSP data because of the longer integration time. No detectable change of signal was seen in FUV data on the egress of gamma Orionis. Clearly, the gas detected at the ingress of the gamma Orionis occultation is not globally distributed. These data are consistent with a plume of gas over the southern pole.
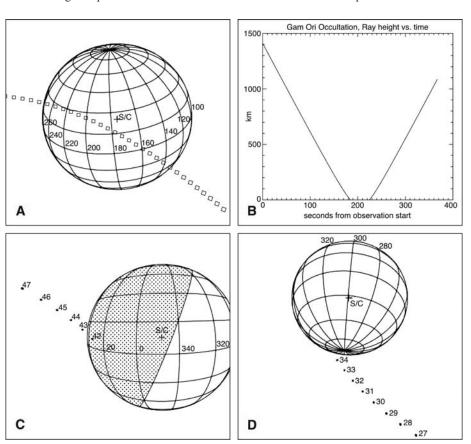
The presence of an absorbing gas shows up in the FUV spectrum as relatively narrow features at short wavelengths and a broad shallow absorption from ∼1450 to 1800 Å as compared to the unocculted spectrum (Fig. 3). Time record 33, the last full 5-s integration before ingress, shows the deepest absorption. The ray altitude above Enceladus' surface corresponding to time record 33 ranged from 30 to 7 km.

The average unocculted star spectrum (I_0) was computed from 25 time records summed over three spatial rows (the instrument pointing drifted slightly over the course of the occultation).

The ratio of time record 33 (I) to I_0 shows the spectrum of the absorbing gas (Fig. 4). We fit the spectrum to water by computing $I = I_0 \exp(-n \times \sigma)$ for water, where σ is the cross section as a function of wavelength (10) and n is the column density. Figure 4 compares a water spectrum with column density $n = 1.5 \times 10^{16}$ cm^{-2} to the I/I_0 spectrum for time record 33. This column density represents the integrated effect of water vapor along the ray path from the spacecraft to the star through the atmosphere. Statistical analysis of smoothed data shows that the water vapor absorption exceeds 2σ beginning with time record 29. The slight mismatch at short wavelengths may be due to using absorption cross sections that were

measured at room temperature [the absorption cross sections at longer wavelengths, which dominate our fit, are not as affected by temperature (11)] and/or imprecise simulation of the instrument response at these wavelengths.

A molecule not apparent in the FUV absorption spectrum is CO. The Cassini Ion Neutral Mass Spectrometer detected a constituent with a mass of 28 atomic mass units, which could be N_2 or CO (12). The Cassini UVIS observation, however, sets an upper limit of $< 1.3 \times 10^{14}$ cm^{-2} from the absence of CO absorption bands (13) at 1544, 1510, 1477, and 1447 Å, assuming that a 10% dip in the signal is required for positive identification of an absorption feature.
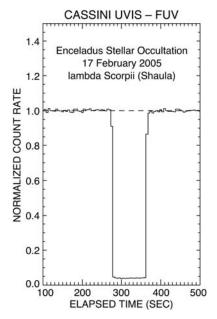

Fig. 1. (**A**) The path followed by the star lambda Scorpii as it was occulted by Enceladus, the first occultation observed by UVIS. The second stellar occultation observed was that of the star gamma Orionis. The altitude of the ray between UVIS and the star relative to the surface of Enceladus is given in kilometers as a function of time in (**B**). The path of gamma Orionis goes from right to left as a function of time in (C) and (D). (**C**) Egress of gamma Orionis. (**D**) Ingress of gamma Orionis. The UVIS field of view is plotted every 5 s. The number over the field of view is the time record number of the data set.
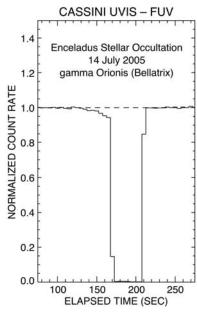
Table 1. Occultation geometry summary.

Occultation date		Occultation intercept latitude	Occultation intercept longitude (west)	Atmosphere detected?
17 February 2005	Ingress	15	300	No
	Egress	−31	141	No
14 July 2005	Ingress	−76	86	Yes
	Egress	−0.20	28	No

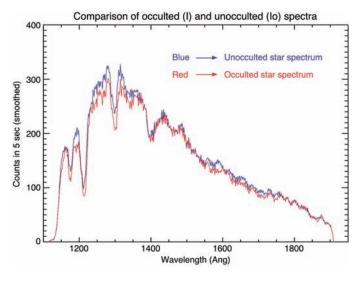**Fig. 2.** The signal of the star plotted versus time for the two occultations observed by UVIS. The left panel shows the steep drop in the FUV count rate as the star lambda Scorpii went behind Enceladus, then reemerged. Similarly, the right panel shows the FUV data from the gamma Orionis occultation. The gradual drop of the signal during ingress is due to the starlight being attenuated by Enceladus' plume. Small steps in the signal on both stars' ingress and egress correspond to the records in which the star was not in the FUV field of view (coming in and/or out of occultation) for the full 5-s integration.
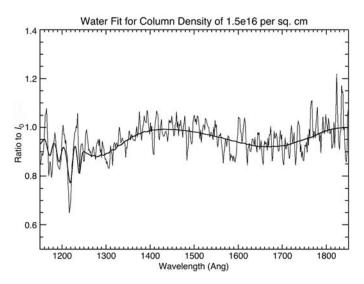

Fig. 3. Smoothed FUV spectra for the unocculted star signal (blue) compared to the signal coming through the plume (red).

Fig. 4. An average unocculted star spectrum (I_0) was computed from 25 time records. The ratio of time record 33 (I) to I_0 is shown (thin line). A water spectrum with column density $n = 1.5 \times 10^{16}$ cm^{-2} divided by I_0 is compared (thick line).

Looking at the slant column abundance of the water vapor versus altitude (Fig. 5), the attenuation of the star signal during the gamma Orionis ingress is best fit with an exponential decline with altitude. The best fit scale length, L, is 80 km. (Because this is an escaping atmosphere, this scale is not the same as the scale height for a gravitationally bound atmosphere.) Time records 27 and 28 appear to show the presence of water, although not yet at a 2σ confidence level.
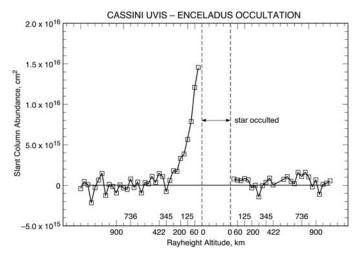
The rate of water loss from Enceladus, S, is given by the product of the molecular abundance N ($= n/h$), the plume area h^2, and the velocity v, as follows: $S = N \times h^2 \times v = n \times h \times v$. We estimate the linear dimension of the plume, h, as the measured scale length $L = 80$ km. The observed column density along the path to the star is $n = 1.5 \times 10^{16}$ cm^{-2}. If we assume that the density corresponds to vapor that is in vapor pressure equilibrium with a warm ice source, then the temperature (T) of the ice is ~145 K. A lower limit for the velocity is the thermal velocity at $T = 145$ K, which gives $v = 41,200$ cm/s. Note that v is well above the 24,000 cm/s escape velocity. The flux is thus at least $S = 5 \times 10^{27}$ molecules/s. Under these simple assumptions, the amount of water escaping from Enceladus is ~ 150 kg/s. Alternatively, h can be estimated from the horizontal dimension of the plume crossed by the star during the course of the occultation, ~175 km. Analysis by the Cassini Composite Infrared Spectrometer team of their thermal data indicates that temperatures could be as high as 180 K (14). At 180 K, the thermal velocity v is 46,000 cm/s. Using $h = 175$ km and $v = 46,000$ cm/s gives $S > 1 \times 10^{28}$ molecules/s, which is approximately 350 kg/s.

Saturn's E ring, composed of water ice grains that are primarily 0.3 to 3 μm in size (15), ex-

Fig. 5. Water abundance shown as a function of time (ticks are every 10 s), labeled with the ray height in kilometers at a few representative times.

CASSINI UVIS – ENCELADUS OCCULTATION

tends from about three to at least eight Saturn radii, with a peak density at Enceladus' orbit (2). Analysis by Jurac et al. (16) concluded that the lifetimes of 1-μm grains are <50 years, because water molecules are sputtered from the grains' surfaces by the plasma trapped in Saturn's magnetosphere. A source of water is needed to maintain the E ring.

Saturn's system is filled with neutral products from the electron- and photodissociation of H_2O molecules: Hubble Space Telescope observations detected neutral OH (17), and UVIS detected neutral atomic oxygen throughout Saturn's system (18) as the Cassini spacecraft approached Saturn. Most H_2O molecules dissociate to $H + OH$, with more O coming from the subsequent dissociation of OH. Neutrals are lost from the system because of charge exchange and collisions with ions. From measured O and OH abundances and theoretical estimates of the loss processes of all water products from the system, various investigators have estimated H_2O supply rates necessary to maintain a steady state as $>2 \times 10^{27}$ H_2O molecules/s (17), possibly as high as 3.75×10^{27} (19) or 10^{28} H_2O molecules/s (20, 21). Potential H_2O sources identified by these investigators included sputtering and collisions; however, the rates of these processes are not sufficient to replace the lost neutrals (19). The source for resupplying the E ring and replacing the neutrals remained a mystery until the discovery of the water vapor plume coming from Enceladus.

The inferred source rate of H_2O in the present observation is of the same order as the earlier estimated loss rates for O and OH. If Enceladus is responsible for the majority of water product gas in the magnetosphere, this implies eruptive activity over at least the past 15 years. The escape flux of water from Enceladus' plume calculated from our measurement of the column density may or may not represent a steady state, because the observation history is confined to a single flyby. Based simply on source magnitude, however, it is probable that Enceladus is the dominant source of the observed neutrals in the Saturn system.

If Enceladus is a significant source for maintaining the E ring, it implies that grain particles are part of the mix of matter in the plume. If Enceladus' plume has a comet-like dust-to-gas ratio, then the mass of water coming from Enceladus, >150 kg/s, is more than sufficient to compensate for the estimated loss rate of the E ring of 1 kg/s (22). The polar plume at Enceladus is clearly an unusual and important geophysical phenomenon.

References and Notes
1. B. A. Smith et al., Science **215**, 504 (1982).
2. M. R. Showalter, J. N. Cuzzi, S. M. Larson, Icarus **94**, 451 (1991).
3. R. J. Terrile, A. Cook, Lunar Planet. Sci **12** (suppl. A), 10 (1981).
4. B. J. Buratti, Icarus **75**, 113 (1988).
5. M. Horanyi, J. A. Burns, D. P. Hamilton, Icarus **97**, 248 (1992).
6. L. Esposito et al., Space Sci. Rev. **115**, 299 (2004).
7. M. K. Dougherty et al., Science **311**, 1406 (2006).
8. J. Saur, D. F. Strobel, Astrophys. J. **620**, L115 (2005).
9. G. R. Smith, D. M. Hunten, Rev. Geophys. **28**, 117 (1990).
10. W. F. Chan, G. Cooper, C. E. Brion, Chem. Phys. **178**, 387 (1993).
11. R. Harrevelt, M. C. Hemert, J. Chem. Phys. **114**, 9453 (2001).
12. J. H. Waite Jr. et al., Science **311**, 1419 (2006).
13. M. Eidelsberg, F. Rostas, J. Breton, B. Thieblemont, J. Chem. Phys. **96**, 5585 (1992).
14. J. R. Spencer et al., Science **311**, 1401 (2006).
15. P. D. Nicholson et al., Science **272**, 509 (1996).
16. S. Jurac, R. E. Johnson, J. D. Richardson, Icarus **149**, 384 (2001).
17. D. P. Shemansky Matheson, D. T. Hall, H.-Y. Hu, T. M. Tripp, Nature **363**, 329 (1993).
18. L. W. Esposito et al., Science **307**, 1251 (2005).
19. S. Jurac et al., Geophys. Res. Lett. **29**, 2172 (2002).
20. S. Jurac, J. D. Richardson, J. Geophys. Res. **110**, A09220 (2005).
21. D. Shemansky et al., paper presented at the meeting of the Committee on Space Research, Paris, France, 18 July 2004.
22. A. Juhasz, M. Horanyi, J. Geophys. Res. **107**, 1066 (2002).
23. This work was partially supported by the Jet Propulsion Laboratory, California Institute of Technology, under a contract with NASA. We thank N. Strange for his efforts in ensuring that the gamma Orionis occultation was included in the design of Cassini's trajectory past Enceladus.

REPORT

Composition and Physical Properties of Enceladus' Surface

Robert H. Brown,[1] Roger N. Clark,[2] Bonnie J. Buratti,[3] Dale P. Cruikshank,[4] Jason W. Barnes,[1] Rachel M. E. Mastrapa,[4] J. Bauer,[3] S. Newman,[3] T. Momary,[3] K. H. Baines,[3] G. Bellucci,[5] F. Capaccioni,[6] P. Cerroni,[6] M. Combes,[7] A. Coradini,[6] P. Drossart,[7] V. Formisano,[5] R. Jaumann,[8] Y. Langevin,[9] D. L. Matson,[3] T. B. McCord,[10] R. M. Nelson,[3] P. D. Nicholson,[11] B. Sicardy,[7] C. Sotin[12]

Observations of Saturn's satellite Enceladus using Cassini's Visual and Infrared Mapping Spectrometer instrument were obtained during three flybys of Enceladus in 2005. Enceladus' surface is composed mostly of nearly pure water ice except near its south pole, where there are light organics, CO_2, and amorphous and crystalline water ice, particularly in the region dubbed the "tiger stripes." An upper limit of 5 precipitable nanometers is derived for CO in the atmospheric column above Enceladus, and 2% for NH_3 in global surface deposits. Upper limits of 140 kelvin (for a filled pixel) are derived for the temperatures in the tiger stripes.

Saturn's sixth largest satellite, Enceladus, orbits the planet within the extended E ring at a distance of 238,040 km, or ~4 Saturn radii. Enceladus has an equatorial diameter of 504.2 km and a surface that consists of a composite of moderately cratered terrain and large expanses with no craters (1). Internal activity has resulted in several episodes of resurfacing, ridge building, folding, and faulting (2, 3). Near-infrared spectroscopy of Enceladus from Earth-based telescopes (4–6) has revealed partially crystalline H_2O ice, consistent with Enceladus' unusually high reflectance. At wavelength 0.8 μm, the geometric albedo slightly exceeds 1.0 (5).